DETECTION OF LUMEN AND MEDIA-ADVENTITIA BORDERS IN IVUS IMAGES USING SPARSE AUTO-ENCODER NEURAL NETWORK

Shengran Su[1,2] Zhifan Gao[2,3*] Heye Zhang[2] Qiang Lin[1+] William Kongto Hau[4] Shuo Li[5]*

1 College of Sciences, Zhejiang University of Technology, China
2 Shenzhen Institutes of Advanced Technology, Chinese Academy of Sciences, China
3 Shenzhen College of Advanced Technology, University of Chinese Academy of Sciences, China
4 LiKaShing Faculty of Medicine, University of Hong Kong, China
5 University of Western Ontario, Canada

ABSTRACT

This paper describes an artificial neural network (ANN) method that employs a feature-learning algorithm to detect the lumen and MA borders in intravascular ultrasound (IVUS) images. Three types of imaging features including spatial, neighboring, and gradient features were used as the input features to the neural network, and then the different vascular layers were distinguished using two sparse autoencoders and one softmax classifier. To smooth the lumen and MA borders detected by the ANN method, we used the active contour model. The performance of our approach was compared with the manual drawing method and another existing method on 538 IVUS images from six subjects. Results showed that our approach had a high correlation (r = 0.9284 ~ 0.9875 for all measurements) and good agreement (bias = 0.0148 ~ 0.4209 mm) with the manual drawing method, and small detection error (lumen border: 0.0928±0.0935 mm, MA border: 0.1056±0.1088 mm). The average time to process each image was 14±4.6 seconds. The obtained results indicate that our proposed approach can be used to efficiently and accurately detect the lumen and MA borders in IVUS images.

Index Terms—Intravascular image, Deep neural network , Image segmentation, Sparse autoencoder

1. INTRODUCTION

Stenosis of the coronary artery caused by the atherosclerosis can lead to clinical complications such as angina, myocardial infarction, and even sudden cardiac death. Cardiovascular diseases are a major health concern since they account for 30% of all deaths worldwide. Intravascular ultrasound (IVUS) technique has been widely applied for diagnosing arteriosclerotic disease of coronary artery over the past decade [1] due to its capability of visualizing the inner structure of blood vessels in real time [2,3]. Compared with other angiographic imaging modalities such as X-ray, magnetic resonance angiography, and computed tomography, IVUS enables the visualization of both vessel morphology and plaque. The extremely high image resolution (up to 113 um) made it be the only modality enabling the accurate morphological segmentation of both vessel membranes (lumen and media) and the assessment of the plaque type in vivo [13, 14]. An important task in the IVUS diagnosis is to determine the plaque burden, which requires the location of lumen border and the media-adventitia (MA) borders of blood vessel [4]. Because of high volume of IVUS images, it could be very challenging to process the IVUS image in real time if the medical physicians need to identify these two borders by hand. Furthermore, high inter-observer and intra-observer variability (up to 20%) might occur in the medical physicians without enough experiences [5]. Therefore, it is a great demand to develop the computer-aided approach to detect the lumen and MA borders for efficient diagnostic and treatment of arteriosclerotic disease.

Most of previous attempts to detect the lumen and MA borders could be divided into three categories: active contour-based method, edge-based method, and probability-based method. The snake and the level set were two commonly used active contour-based methods for border detection [6], however, the contour evolution was heavily depend on the prior shape constraints of blood vessel. In the contrast, the edge-based method detects the borders by analyzing the appearance of edges in the IVUS images [7]. The region-based method detects the borders by distinguishing the lumen region, plaque region and adventitia region using appearance difference among the three regions [8]. Nevertheless, the performance of these three methods highly relied on sophisticated features that might only work for specific problem. For example, in the active contour-based method, gradient vector flow is usually to deal with the problem of boundary concavities [9]. For the edge-based method and region-based method, it is challenging to design proper edge features or region features in order to recognize the lumen and MA interfaces [6]. Therefore, the results are often dependent on the choice of

* *Mr. Shengran Su and Mr. Zhifan Gao contributed equally to this work.*
+*Corresponding Author: Dr. Qiang Lin (qlin@zjut.edu.cn)*

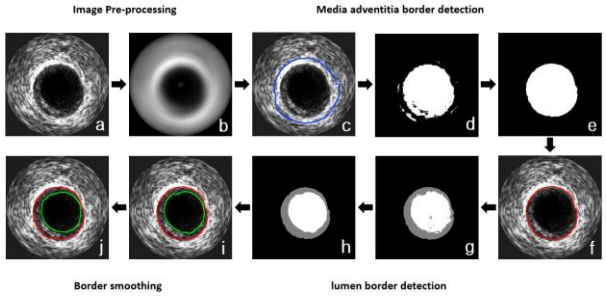

Fig.1. The flowchart of our approach: (a) the original image; (b) the image after using the mean filter; (c) the ROI region within the blue curve; (d) the result after the first ANN in detecting the MA border; (e) the result after the second ANN in detecting the MA border; (f) MA border labeled by the red contour; (g) the result after the first ANN in detecting the lumen border; (h) the result after the second ANN in detecting the lumen border; (i) lumen border labeled by the red contour; (j) the smoothed borders.

features. If there is a method based on universal features, such as pixel and gradient information, it may greatly enhance the robustness and accuracy of the method. In this work, we apply the artificial neural network (ANN) method to learn the hidden structures and connections of general imaging features and transform them into a more efficient representation. We use these three imaging features including spatial feature, neighborhood feature and gradient feature as the input to the ANN method. Our approach has been tested on a set of 538 IVUS images from six subjects by comparing to the manual drawing method and one existing detection method [10].

2. METHODOLOGY

An ANN is a popular algorithm used in classification and regression problems, and it can extract hidden structures and connections among image features by learning their compressed representation. In this study, we applied the ANN method to learn imaging features in order to detect the lumen and MA borders in IVUS images [11]. After learning imaging features of different vessel layers using the ANN method, we could identify the borders by distinguishing different regions of a blood vessel. Fig.1 shows the steps involved in our approach.

2.1. Preprocessing

Before learning the imaging feature, the original IVUS images are smoothed in polar coordinates by a mean filter with size of 71×31 pixels, and then transformed back into Cartesian coordinates (Fig.1(b)). The brightest pixels in every radial direction are connected as one closed contour, and the region inside this contour will be used the ROI for the following imaging feature learning (Fig.1(c)).

2.2. Artificial neural network

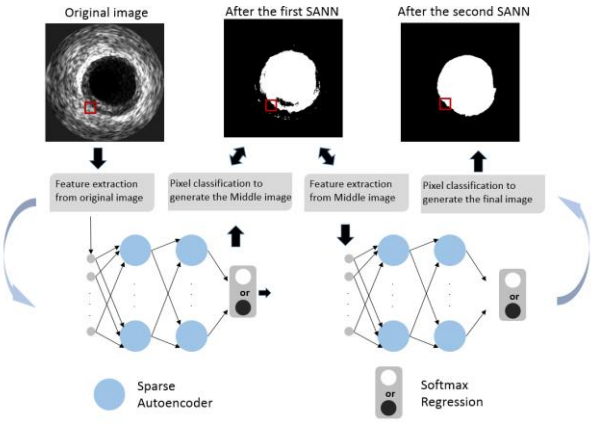

Fig.2. Double SANN structure. The first SANN classifies the pixels coarsely, and the second SANN are used to optimize the results of the first network.

The proposed ANN consists of two sparse autoencoder artificial neural network (SANN) for coarse-to-fine classify-cation of pixels in the ROI, shown in Fig. 2. The first SANN coarsely classifies the pixels inside the ROI. We define three types of imaging features: spatial features, neighboring features, and gradient features in every pixel inside the ROI. Let p be the pixel inside the ROI, spatial feature fs is the value of polar coordinates of p, defined by $f_s = [r, \theta]$ where r is the distance from pixel p to the IVUS catheter (image center), and θ is the angle in polar coordinates. Neighbouring feature f_n is the distribution of the intensity value around the pixel p. It contains two kinds of neighboring information f_{n1} and f_{n2} in two difference image scales. For f_{n1}, the neighbourhood of p, 15×15 pixels, is equally divided 9 blocks, and the size of each block is 5×5 pixels. Then f_{n1} can be formulated as $f_{n1} = [m_1, m_2, \dots m_9]$, where m_i $(i = 1,2, \dots ,9)$ is the mean values of pixels in the ith block. f_{n2} is the 8-neighbouring pixels around the p. The gradient feature f_g is the imaging gradient along the radial direction at the location of p. Thus, the feature f extracted from one pixel could be obtained by $f = [f_s, f_n, f_g]$. The dimension of all the imaging features is 21 in this work, and thus the number of elements in the input vector to the SANN was 21N, where N is the pixel number in the ROI (Fig.1(c)). After using the first SANN, we can have one binary image B that has the same size as the original IVUS image (Fig. 2). We will use the second SANN to refine the results of classification in the first SANN. In the second SANN, the imaging feature f_n of every pixel in the binary image B is used to divide the pixels within B into two categories. We consider that we trained two SANNs to extract the boundary. The first network implements a coarse classification function, and the second network optimizes the results of the first network to as to remove noise (Fig.1(e)). The method involves first finding

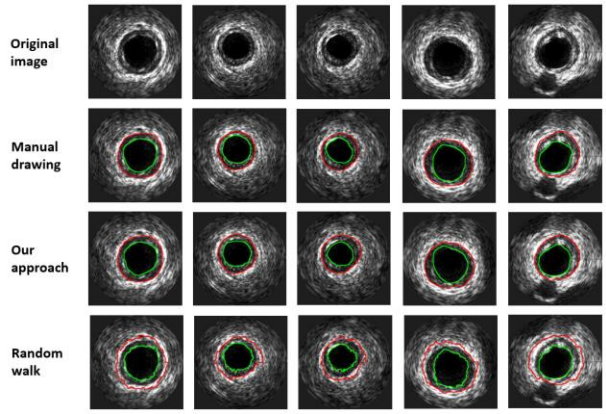

Fig.3. Example results of detecting the lumen and media-adventitia borders. The first row contains the original IVUS images. The second, third and fourth rows contain the IVUS images with results from the manual drawing method, the propose method and the previous method (Random walk). The red curve is the media-adventitia border and the green curve is the lumen

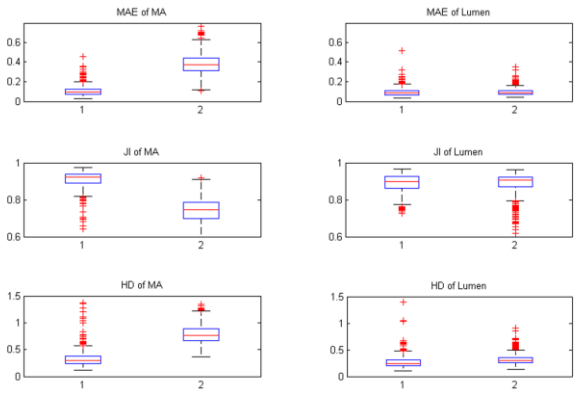

Fig.4. Box plots show the errors of MAE, JI and HD. 1 means our approach and 2 means Random Walk method.

the MA boundary by classifying pixels inside or outside this boundary. The same method is then used to find the lumen boundary only in the region inside the MA boundary.

2.3. Postprocessing

In order to obtain smoothed lumen and MA borders, we use the active contour model [9] to polish the borders generated by the ANN method. The lumen and MA borders detected by ANN are used to initialize the active contour model.The coefficients of the tension term and stiffness term in the internal energy were set 10 and 0.1, respectively. The weight values of lines and edges and terminations in the potential energy were set -0.5, 5, and 1, respectively. The smoothed lumen and MA borders can be seen in Fig. 1(j).

3. EXPERIMENTS AND RESULTS

In order to validate the performance of our approach, our approach was compared to the manual drawing method and another existing method on 538 IVUS images from six subjects. The following content will explain the details of all the experiments in this work.

3.1. Data Collection

All the IVUS data were collected using a commercially available IVUS machine (In-Vision Gold, Volcano) with a 20 MHz solid-state IVUS catheter (EagleEye Volcano). The IVUS catheter was advanced >5 mm distal to the target lesion, and then pulled back with speed of 0.5 mm/s using an automatic pullback device (R-100, Volcano) for recording IVUS data. All the imaging data then were saved on CDs in DICOM format into CDs for off-line analysis. A total of 598 IVUS images from six subjects were used in this study, where 60 IVUS images were applied for Double SANN training and 538 IVUS images were used for performance evaluation of the proposed approach. These IVUS images were chosen by one IVUS expert with 25 year-experience according to predefined selection criteria of the state of atherosclerosis in the subjects: the recruited subjects had moderate or mild atherosclerosis, and every selected IVUS image without bifurcations, stents, dense calcification with acoustic shadowing and other complex lesions. Each participant was informed of the purpose and procedure of this study. Informed consent was obtained from each participant. All data in this study were analyzed using Matlab R2012a on a desktop computer with Intel(R) Xeon(R) CPU E5-2650(2.00 GHz) and 32GB DDR2 memory.

3.2. SANN Training

The training set (denoted by Train1) includes 60 IVUS images, which were equally selected from all six subject by the expert. Other images in the dataset were used for the model testing. In the training of the first SANN, all pixels in the IVUS image are assigned to two labels (vessel and non-vessel). Then the greedy-wise training method is used to train the SANN. In the greedy-wise training, we trained M times for the SANN with M layers. It considers the output of the k layers ($k = 1, \dots, M$) we have just trained as the input of the k+1th layer we are about to train. Finally, the weight of each unit on the SANN is finetuned with the back propagation algorithm in order to determine the weights of all units on the first SANN. The training of the second SANN is same with that of the first SANN, except that the pixels are assigned to two different labels (lumen and non-lumen). Additionally, in order to validate the influence on the performance of our approach from the correlation among the training images from the same subject, we used another scheme to select the images in the training set. In this scheme, all images from two subjects were considered as the training set (denoted by Train2), and images from other four subjects formed the corresponding test set. The training process for Train2 are same with that for Train1. Table 1 lists the test errors based on the parameters of the ANN

Lumen	Train1	Test1		Train2	Test2		Random walk
	–	SANN	SANN+AC	–	SANN	SANN+AC	–
MAE	0.1296±0.2360	0.0966±0.0989	0.0928±0.0935	0.0924±0.0887	0.0882±0.1037	0.0819±0.0936	0.098±0.04
HD	0.4546±0.5740	0.3035±0.1816	0.2732±0.1595	0.2970±0.1131	0.2996±0.2091	0.2612±0.1826	0.325±0.128
JI	81.41±12.61	88.65±4.91	88.87±5.15	89.09±3.71	89.59±5.39	90.21±5.47	88.64±5.89

MA	Train1	Test1		Train2	Test2		Random walk
	–	SANN	SANN+AC	–	SANN	SANN+AC	–
MAN	0.1278±0.1478	0.1141±0.1283	0.1056±0.1088	0.0881±0.0917	0.1369±0.1462	0.1196±0.1203	0.3804±0.1107
HD	0.4910±0.2700	0.3877±0.2244	0.3327±0.1657	0.3140±0.1600	0.4291±0.2238	0.3529±0.1705	0.7870±0.1714
JI	88.15±5.47	90.14±5.24	90.93±4.50	92.38±3.56	88.48±6.35	89.89±5.36	73.95±7.09

Table 1. Training errors and test errors measured by the mean absolute error (mm), Hausdorff distance (mm) and Jaccard Index (%). The column "Train1" shows the training errors computed on the training set "Train1" and "Test1" shows the corresponding test errors. The column "Train2" shows the training errors computed on the training set "Train2" and "Test2" shows the corresponding test errors. "SANN" means that our approach only uses the SANN, "SANN+AC" means that our approach use the combination of the SANN and the active contour, and "Random walk" means that the Random walk method .

trained by Train1 and Train2. The results show that there is little difference when the two training sets are used. Thus we can conclude that performance of our approach is little influenced by the correlation among the training images from the same subject.

3.3. Accuracy:

The accuracy of our approach was evaluated by comparing to the manual trace results performed by one IVUS expert with 25 year-experience (considered as the ground truth). We use eight measures to evaluate the accuracy of our approach: lumen cross-sectional area (LCSA), minimum lumen diameter (MinLD), maximum lumen diameter (MaxLD), plaque plus media CSA (PCSA), plaque burden (PB), vessel cross-section area (VCSA), minimum vessel diameter (MinVD), maximum vessel diameter (MaxVD), The first six measurements were suggested by the American College of Cardiology consensus statement on IVUS [12]. The results show that the correlation coefficients of linear regression between our approach and manual drawing method are 0.9875 mm (LCSA), 0.9763 mm (MaxLD), 0.9804 mm (MinLD), 0.9736 mm (VCSA), 0.9578 mm (MaxVD), 0.9474 mm (MinVD), 0.9284 mm (PCSA) and 0.9510 mm (PB), and all the p-values were smaller than 0.001. This means that our results are highly correlated to the ground truth. The Bland-Altman analysis shows that the average bias between our approach and the manual drawing method were 0.1713 mm (LCSA), 0.0334 mm (MaxLD), -0.0012 mm (MinLD), 0.2497 mm (VCSA), 0.0969 mm (MaxVD), 0.0231 mm (MinVD), 0.4209 mm (PCSA), 0.0148 mm (PB). And >99.26% results of the Bland-Altman analysis are within the 95% confidence interval for all measurements. These results indicate that our approach are well agreed with the manual drawing method. In addition, Then Table 1 shows the detection error of our approach measured by the mean absolute error (MAE), Hausdorff distance (HD) and Jaccard index (JI). The accuracy demonstrates that our approach might have great potential in the analysis of inner vascular structure for clinical diagnosis. In addition, we computed that contribution of SANN and active contour to the overall results. Table 1 displays that the active contour slightly improves the performance of our approach, and it mainly contributes to the border smoothness.

3.4. Compared with the other method

Our approach was compared with one recent method (random walk) [10]. The code is generated by ourselves. The error of our approach is 0.0928±0.0935 mm for the lumen border and 0.1056±0.1088 mm for the MA border, while the error of the random walk algorithm is 0.0944± 0.0921 mm for the lumen border and 0.3811±0.2255 mm for the MA border. Our approach shows higher accuracy than this random walk method (Fig.4).

4. CONCLUSION

In this study, we developed an approach to detect the lumen and MA borders from IVUS images using the sparse auto-encoder neural network. The proposed approach has been evaluated on 538 IVUS images acquired from six subjects by comparing to the manual drawing method and one existing computer-aided method. The experimental results showed that our approach was well correlated and agreed with manual drawing method.

5. ACKNOWLEDGEMENTS

This study was supported by the 973 Program of China (2013CB329501) and the National Natural Science Foundation of China (61475139).

6. REFERENCES

[1] E. Brunenberg, O. Pujol, B. Romeny, and P. Radeva, "Auto-

matic IVUS segmentation of atherosclerotic plaque with stop & go snake," International Conference on Medical Image Computing and Computer Assisted Intervention (MICCAI), 2006.
[2] F. Ciompi, O. Pujol, E. Fern´andez-Nofrer´ıas, J. Mauri, and P. Radeva, "Ecoc random fields for lumen segmentation in radial artery IVUS sequences," International Conference on Medical Image Computing and Computer Assisted Intervention (MICCAI), 2009.
[3] F. Ciompo, O. Pujol, C. Gatta, X. Carrillo, J. Mauri, and P. Radeva, "A holistic approach for the detection of media-adventitia border in IVUS," International Conference on Medical Image Computing and Computer Assisted Intervention (MICCAI), 2011.
[4] E. Mendizabal-Ruiz, G. Biros, and I. Kaladiaris, "An inverse scattering algorithm for the segmentation of the luminal border on intravascular ultrasound data," International Conference on Medical Image Computing and Computer Assisted Intervention (MICCAI), 2009.
[5] D. Meier, R. Cothren, D. Vince, and J. Cornhill, "Automated morphometry of coronary arteries with digital image analysis of intravascular ultrasound," American Heart Journal, vol. 133, no. 6, pp. 681–690, 1997.
[6] A. Katouzian, E. Angelini, S. Carlier, J. Suri, N. Navab, and A. Laine, "A state-of-the-art review on segmentation algorithms in intravascular ultrasound (IVUS) images," IEEE Transactions on Information Technology in Biomedicine, vol. 16, no. 5, pp. 823–834, 2012.
[7] E. Essa, X. Xie, I. Sazonov, and P. Nithiarasu, "Automatic IVUS media-adventitia border extraction using double interface graph cut segmentation," IEEE International Conference on Image Processing (ICIP), 2011.
[8] E. Mendizabal-Ruiz and I. Kakadiaris, "Prababolistic segmentation of the lumen from intravascular ultrasound radio frequency data," International Conference on Medical Image Computing and Computer Assisted Intervention (MICCAI), 2012.
[9] C. Xu and J. Prince, "Snakes, shapes, and gradient vector flow," IEEE Transactions on Image Processing, vol. 7, no. 3, pp. 359–369, 1998.
[10] J. Yan, H. Liu, and Y. Cui, "A random walk-based method for segmentation of intravascular ultrasound images," SPIE Medical Imaging, 2014.
[11] G. Hilton and R. Salakhutdinov, "Reducing the dimensionaloty of data with neural networks," Science, vol. 5786, no. 313, pp. 504–507, 2006.
[12] G. Mintz, S. Nissen, W. Anderson, S. Bailey, R. Erbel, P. Fitzgerald, F. Pinto, K. Rosenfield, R. Siegel, and E. Tuzcu, "American college of cardiology clinical expert consensus document on standards for acquisition, measurement and reporting of intravascular ultrasound studies (IVUS)," Journal of the American College of Cardiology, vol. 37, no. 5, pp. 1478–1492, 2001.
[13] Nair, Anuja, et al. "Coronary plaque classification with intravascular ultrasound radiofrequency data analysis." Circulation, vol. 106, no. 17, pp. 2200-2206, 2002.
[14] Sathyanarayana, Shashidhar, et al. "Characterisation of atherosclerotic plaque by spectral similarity of radiofrequency intravascular ultrasound signals." EuroIntervention, vol. 5, no. 1, pp. 133-139, 2009.